

Supporting information for:

## Structural stability and thermoelectric properties of cation- and anion-doped $\text{Mg}_2\text{Si}_{0.4}\text{Sn}_{0.6}$

Henrik L. Andersen,<sup>a</sup> Jiawei Zhang,<sup>a</sup> Hao Yin,<sup>b</sup> and Bo B. Iversen<sup>\*a</sup>

<sup>a</sup> Center for Materials Crystallography, Department of Chemistry and iNANO, Aarhus University, DK-8000 Aarhus C, Denmark

<sup>b</sup> TEGnology ApS, Lundagervej 102, DK-8722, Hedensted, Denmark

### Contents

Sample preparation .....	2
SPS reproducibility .....	2
Pre- and post SPS PXRD patterns .....	3
Thermal stability .....	4
Multi-temperature PXRD data .....	4
Thermal stability of SPS-pellets .....	6
References .....	9

## Sample preparation

### SPS reproducibility

An identical preprogrammed SPS procedure was employed in the compaction of all pellets to ensure comparability of the pellets. Figure S1 (A) and (B) show comparisons of PXRD patterns measured on the top and bottom sides of different MGS\_Sb pellets illustrating the excellent reproducibility of the SPS method and comparability of the samples.

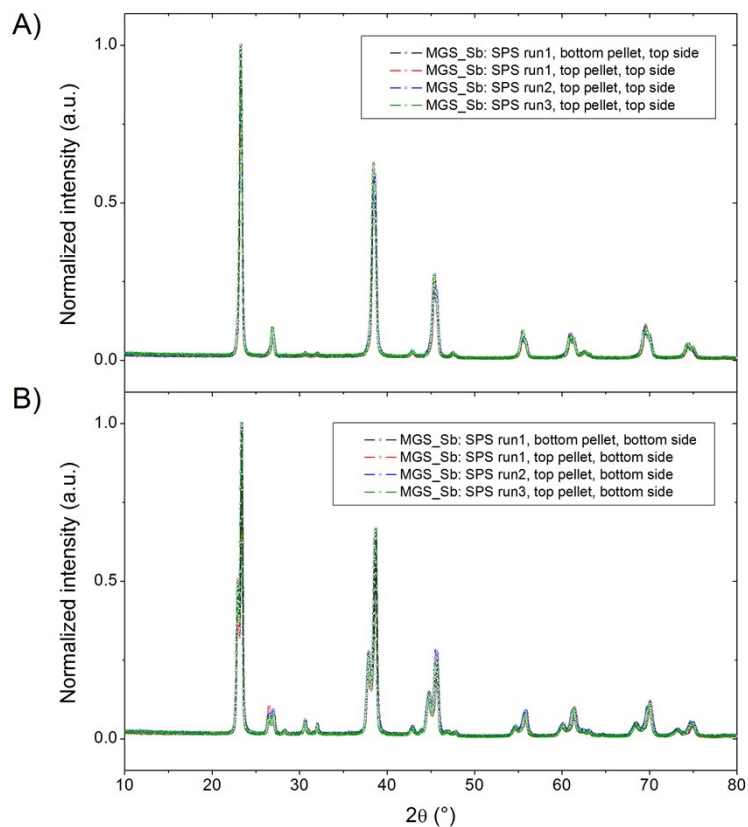


**Figure S1.** Comparison of PXRD patterns from top and bottom sides of different SPS compacted pellets of the MGS\_Sb sample.

The PXRD patterns were collected on an in-house Rigaku SmartLab powder X-ray diffractometer (Rigaku, Japan) using Cu  $K\alpha_{1,2}$  radiation ( $\lambda_1=1.541 \text{ \AA}$ ,  $\lambda_2=1.544 \text{ \AA}$ ). Only very minor and negligible differences between the patterns from the different pellets are observed. The PXRD data also illustrates the consistent formation of the gradient with the peak splitting present in all patterns measured on the bottom side of the pellets.

### Pre- and post SPS PXR patterns

Figure S2 shows representative PXR patterns of the as-synthesized powder, and of the top and bottom sides of pellets of the five different samples. The PXR patterns were collected on an in-house Rigaku SmartLab powder X-ray diffractometer (Rigaku, Japan) using Cu  $K\alpha_{1,2}$  radiation.

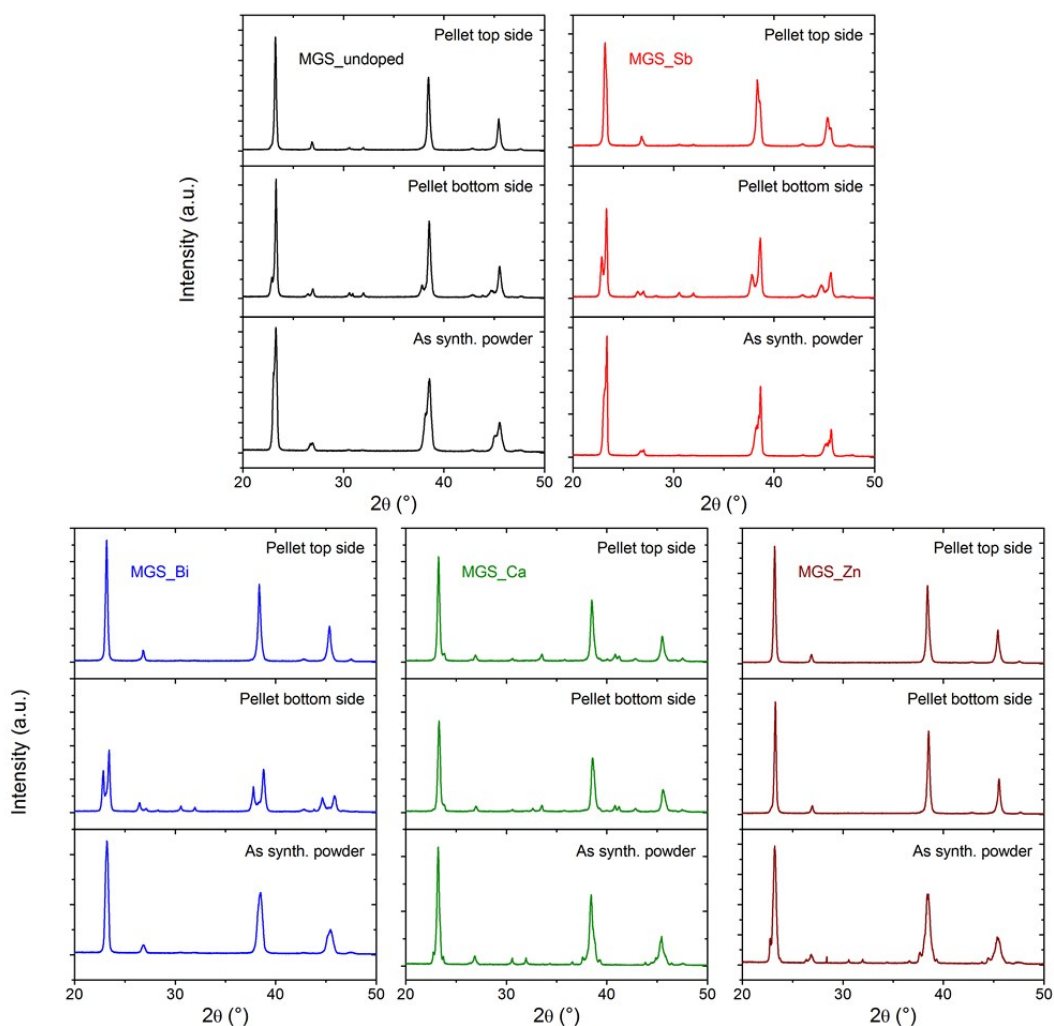


**Figure S2.** PXR patterns of as-synthesized powder, and bottom and top sides of SPS compacted pellets of all five prepared compositions, i.e. MGS\_undoped, MGS\_Sb, MGS\_Bi, MGS\_Ca and MGS\_Zn.

Peak splitting is observed in the patterns measured on the bottom side of the pellets for MGS\_undoped, MGS\_Sb and MGS\_Bi indicating gradient formation. However, cation-doping by Ca and Zn seems prevent the gradient formation as no peak splitting and only a very minor peak asymmetry is observed on either side of the pellets.

## Thermal stability

### Multi-temperature PXRD data

The structural and compositional stability of the samples in the temperature range 300-750K have been characterized by high-resolution synchrotron PXRD at the BL44B2 beamline, SPring-8, Japan, at a wavelength of 0.500443(4) Å.<sup>1</sup> The measurements were conducted on representative powders filed off the entire thickness of the pellets and packed under Ar in  $\varnothing=0.3$  mm (inner diameter) quartz capillaries. Contour plots of the multi-temperature diffraction patterns of the MGS\_undoped, MGS\_Sb, MGS\_Bi, MGS\_Ca, and MGS\_Zn samples are shown in Figure S3, Figure S4, Figure S5, Figure S6, and Figure S7, respectively.

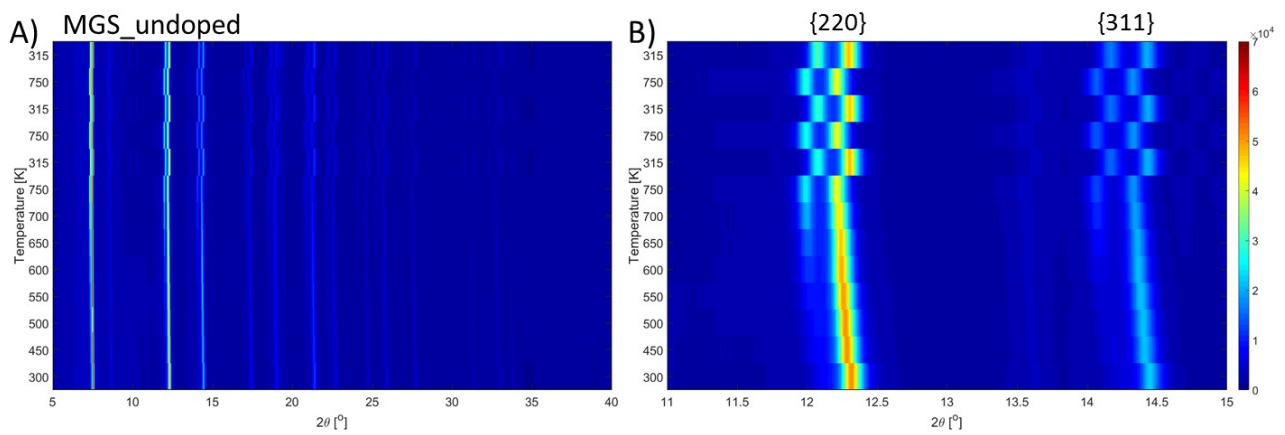


**Figure S3.** A) Multi-temperature high-resolution synchrotron PXRD data of the MGS\_undoped sample. B) Enhancement of selected  $2\theta$ -region illustrating the evolution of the 220 and 311 reflections.

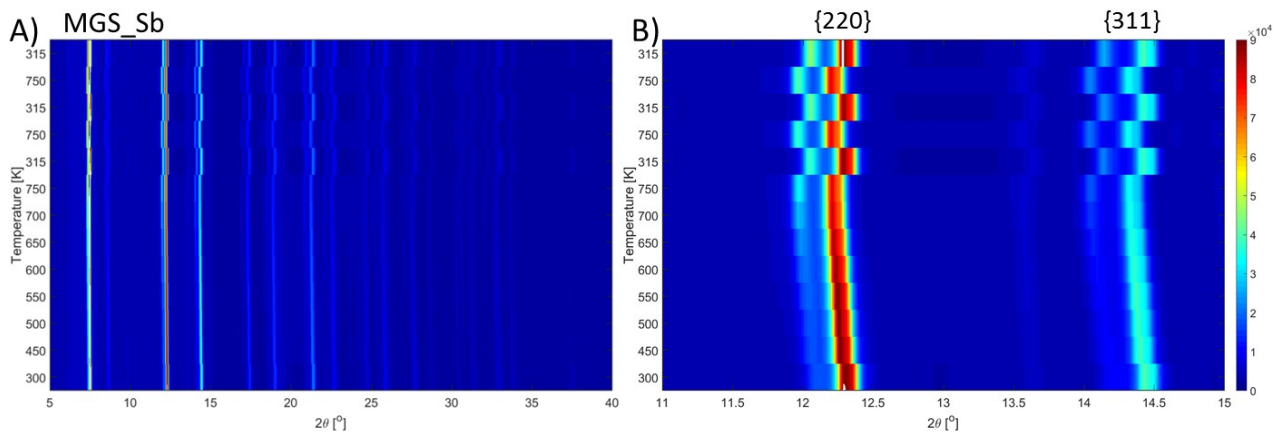


**Figure S4.** A) Multi-temperature high-resolution synchrotron PXRD data of the MGS\_Sb sample. B) Enhancement of selected  $2\theta$ -region illustrating the evolution of the 220 and 311 reflections.

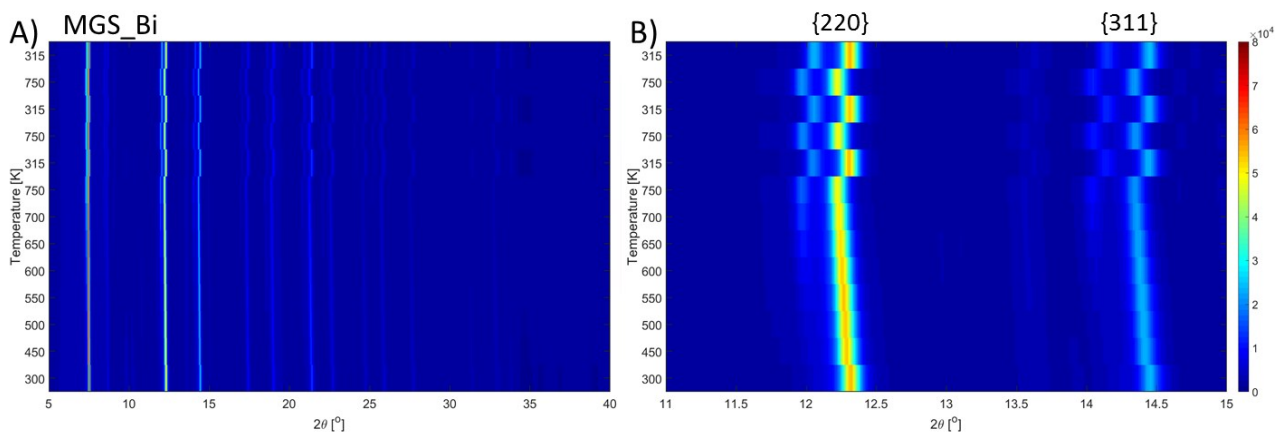


**Figure S5.** A) Multi-temperature high-resolution synchrotron PXRD data of the MGS\_Bi sample. B) Enhancement of selected  $2\theta$ -region illustrating the evolution of the 220 and 311 reflections.

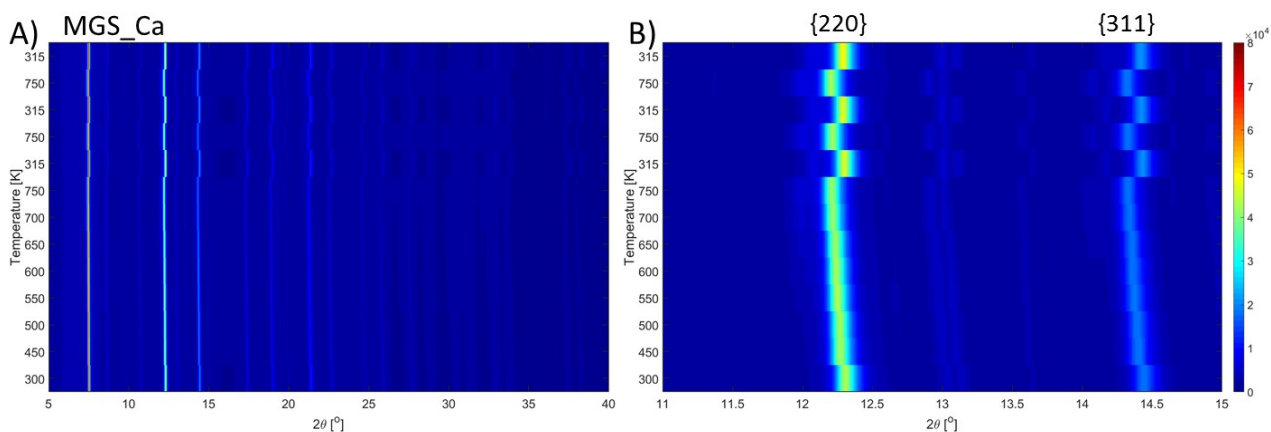


**Figure S6.** A) Multi-temperature high-resolution synchrotron PXRD data of the MGS\_Ca sample. B) Enhancement of selected  $2\theta$ -region illustrating the evolution of the 220 and 311 reflections.

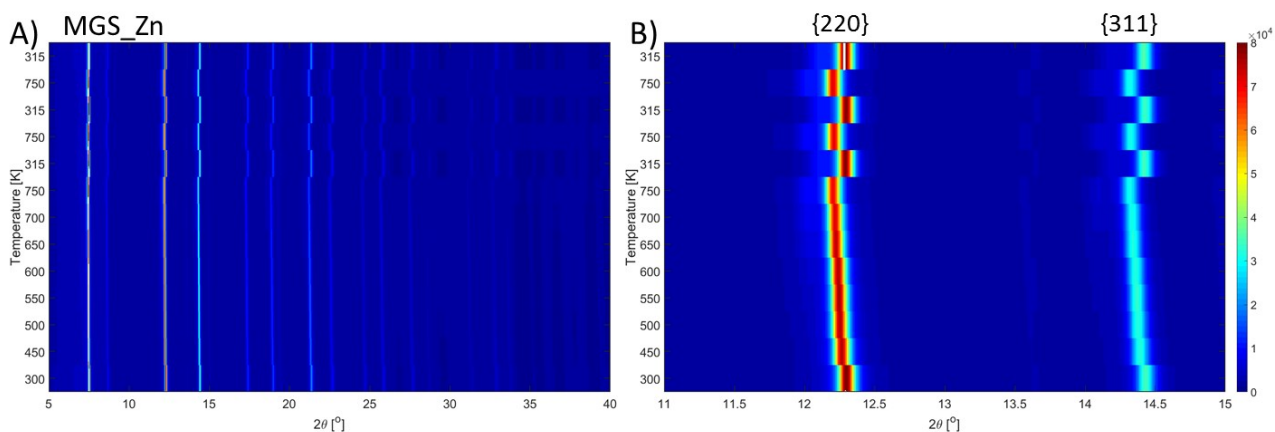


**Figure S7.** A) Multi-temperature high-resolution synchrotron PXRD data of the MGS\_Sb sample. B) Enhancement of selected  $2\theta$ -region illustrating the evolution of the 220 and 311 reflections.

The enhancements of the 11-15°  $2\theta$ -regions shown on the right of the corresponding full patterns illustrate the structural instability and resulting peak splitting in the MGS\_undoped, MGS\_Sb, and MGS\_Bi samples,

along with the structural stability of the MGS\_Ca and MGS\_Zn samples. The enhancements also highlight the thermal expansion of the unit cell, causing a shift to lower  $2\theta$ -angle of the reflections.

### Thermal stability of SPS-pellets

The multi-temperature PXRD data was measured on powder filed off the SPS compacted pellets. However, to test the thermal stability of the pellets themselves, room temperature PXRD data was measured on top and bottom of the sample pellets before and after thermal cycling from 300 to 725 K in vacuum. The PXRD patterns of the MGS\_undoped, MGS\_Sb, MGS\_Bi, MGS\_Ca, and MGS\_Zn samples are shown in Figure S8, Figure S9, Figure S10, Figure S11, and Figure S12, respectively. The PXRD patterns were collected on an in-house Rigaku SmartLab powder X-ray diffractometer (Rigaku, Japan) using Cu  $K\alpha_{1,2}$  radiation.

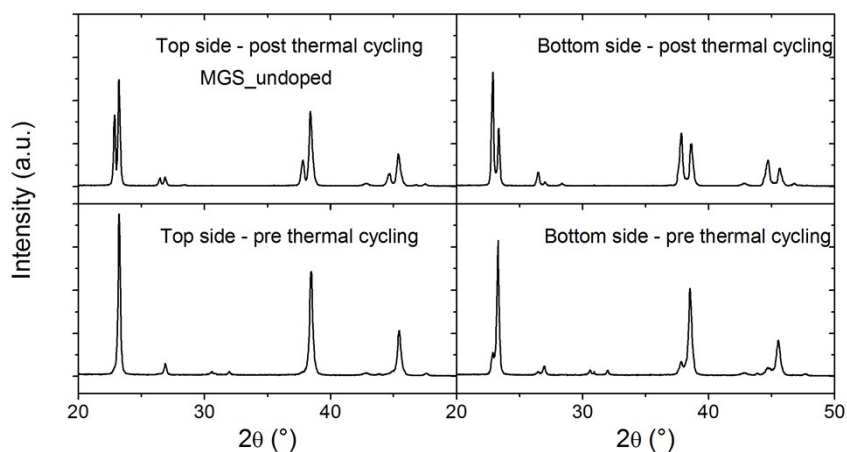


**Figure S8.** PXRD patterns measured on top and bottom of an SPS compacted pellet of MGS\_undoped before and after thermal cycling to 300 to 725K in vacuum.

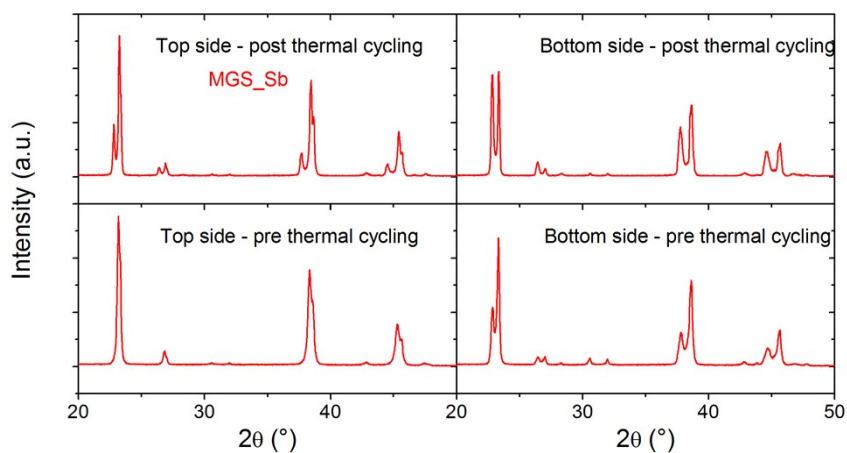


**Figure S9.** PXRD patterns measured on top and bottom of an SPS compacted pellet of MGS\_Sb before and after thermal cycling to 300 to 725K in vacuum.

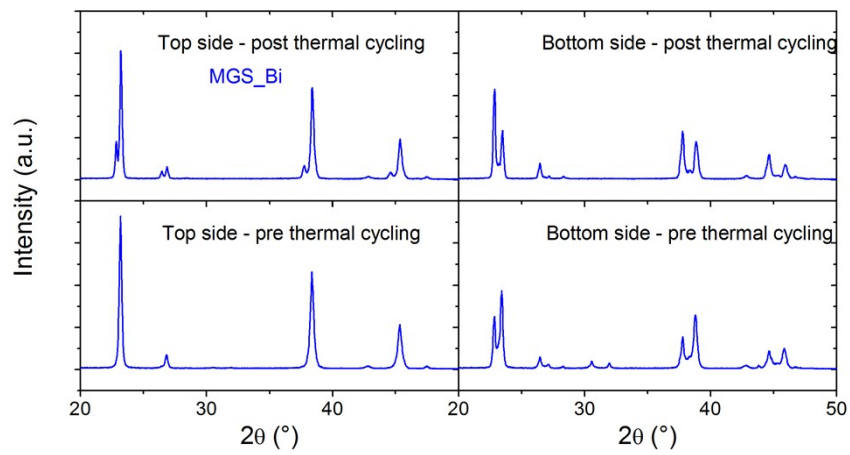


**Figure S10.** PXRD patterns measured on top and bottom of an SPS compacted pellet of MGS<sub>Bi</sub> before and after thermal cycling to 300 to 725K in vacuum.

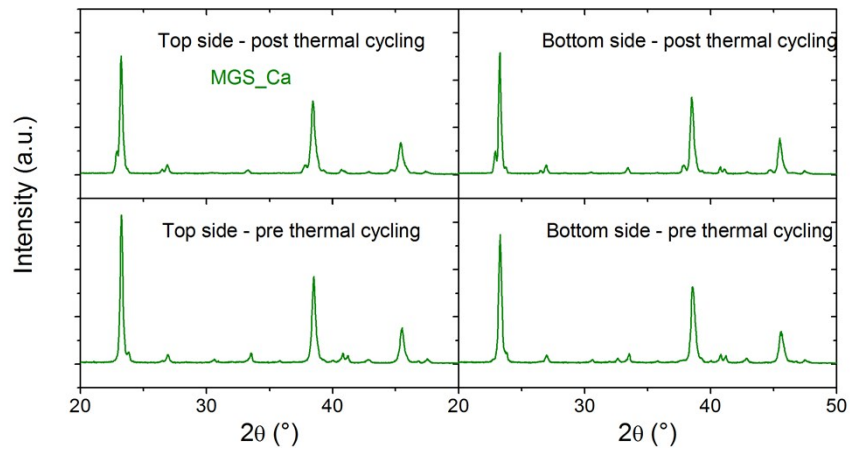


**Figure S11.** PXRD patterns measured on top and bottom of an SPS compacted pellet of MGS<sub>Ca</sub> before and after thermal cycling to 300 to 725K in vacuum.

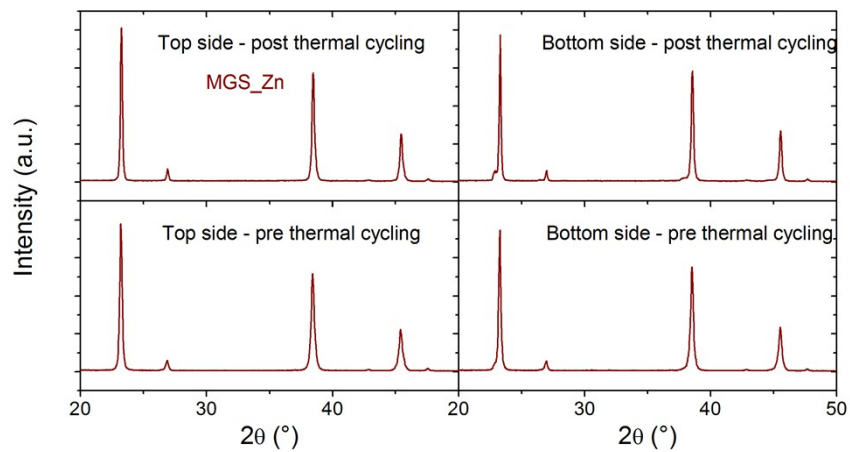


**Figure S12.** PXRD patterns measured on top and bottom of an SPS compacted pellet of MGS\_Zn before and after thermal cycling to 300 to 725K in vacuum.

The PXRD data of the pellets agree very well with the multi-temperature synchrotron PXRD data with significant peak splitting occurring both on the top and bottom sides in the MGS\_undoped, MGS\_Sb and MGS\_Bi samples. Again, only very subtle changes are observed in the PXRD patterns of the MGS\_Ca and MGS\_Zn samples, confirming the stabilizing effect of Ca and Zn doping on the pellets as well.

## Lorenz number calculation

Under the single parabolic band model, the Lorenz number shown in Figure 10(B) is calculated by:<sup>2</sup>

$$L = \left( \frac{k_B}{e} \right)^2 \left\{ \frac{\left( r + \frac{7}{2} \right) F_{r+5/2}(\eta)}{\left( r + \frac{3}{2} \right) F_{r+1/2}(\eta)} - \left[ \frac{\left( r + \frac{5}{2} \right) F_{r+3/2}(\eta)}{\left( r + \frac{3}{2} \right) F_{r+1/2}(\eta)} \right]^2 \right\}, \quad (2)$$

The Fermi integral is given by:

$$F_n(\eta) = \int_0^\infty \frac{\varepsilon^n d\varepsilon}{1 + \exp(\varepsilon - \eta)}, \quad (3)$$

Here  $k_B$  is the Boltzmann constant,  $e$  is the elementary charge, and  $\eta$  is the reduced Fermi energy. The scattering factor  $r = -0.5$  is adopted for the acoustic phonon scattering mechanism.

## References

1. S. Adachi, T. Oguchi, H. Tanida, S. Y. Park, H. Shimizu, H. Miyatake, N. Kamiya, Y. Shiro, Y. Inoue, T. Ueki and T. Iizuka, *Nucl. Instr. Meth. Phys. Res.*, 2001, **467–468, Part 1**, 711.
2. H. J. Goldsmid, *Thermoelectric refrigeration*, Plenum Press, New York,, 1964.